Direction-division multiplexed holographic free-electron-driven light sources

Brendan Clarke[1], Kevin F. MacDonald[1], and Nikolay I. Zheludev[1, 2]

[1] *Optoelectronics Research Centre & Centre for Photonic Metamaterials, University of Southampton, Southampton, SO17 1BJ, UK*

[2] *Centre for Disruptive Photonic Technologies, School of Physical and Applied Sciences & The Photonics Institute, Nanyang Technological University, Singapore 637371*

We report on a free-electron-driven light source with a controllable direction of emission. The source comprises a microscopic array of plasmonic surface-relief holographic domains, each tailored to direct electron-induced light emission at a selected wavelength into a collimated beam in a prescribed direction. The direction-division multiplexed source is tested by driving it with the 30 kV electron beam of a scanning electron microscope: light emission, at a wavelength of 800 nm in the present case, is switched among different output angles by micron-scale repositioning of the electron injection point among domains. Such sources, with directional switching/tuning possible at picosecond timescales, may be applied to field emission and surface-conduction electron-emission display technologies, optical multiplexing and to charged-particle-beam position metrology.

Free-electron-driven light emission[1] is attracting considerable attention for applications in high spatial, spectral and temporal resolution characterization of photonic nanostructures, and in the context of nanoscale frequency-tunable free-electron-driven light sources. A charged particle (in vacuum) impacting a metal surface generates transition radiation[2] (with a highly-divergent spatial distribution) and surface plasmons[3, 4] (that may subsequently couple to free-space light emission), with a spectral distribution and relative intensity related to the relative permittivity of the target and the electron energy. Light can also be generated in 'proximity interactions' between nanostructured materials and the evanescent field of moving electrons as they fly past at sufficiently close range[5, 6]. These emission mechanisms underpin the hyperspectral electron-induced radiation emission (EIRE) imaging techniques that have been developed and applied in recent years to the study of surface plasmon polariton propagation,[7, 8] the mapping of plasmonic nanoparticle resonance modes,[9-11] and the identification of structural phase states.[12, 13] Recent technological developments have facilitated polarization-resolved EIRE spectroscopy[14] and the tomographic visualization of plasmonic modes in 3D core-shell structures.[15] The same emission mechanisms are the foundation of assorted electron-beam-driven nanoscale light sources, wherein the emission wavelength is typically a function of electron energy and nanostructural periodicity.[16, 17]

At the nanoscale, as indeed at all dimensional scales, numerous applications call for active control over not only the wavelength, but also the direction, divergence, and polarization of light emission and/or propagation. A wide variety of photonic crystal, plasmonic and metamaterial/metasurface structures, including dynamically reconfigurable structures,[18, 19] seek to address this challenge. In the particular context of EIRE, it has been demonstrated that plasmonic nanostructures

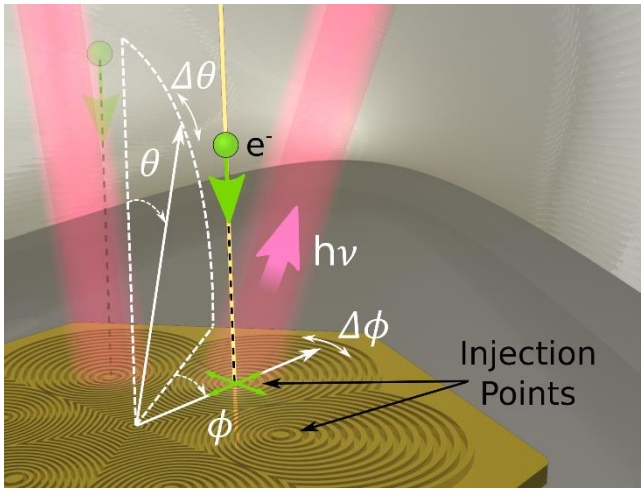

Figure 1. Artistic impression of multiplexed array of free-electron holographic light sources, each engineered to emit light of a chosen wavelength and wavefront profile in particular polar (θ) and azimuthal (φ) directions. The direction of light emission from the ensemble is thereby actively controlled by selectively targeting individual sources with a scanning electron beam pump, and fine-tuned ($\pm\Delta\theta$, $\Delta\varphi$ as much as 15º) for each source via nanometer-scale variations in the electron injection position around the target point.

(from nano-antennas to cylindrical 'undulators' and metasurface resonator arrays) can couple medium-energy free-electron excitations to free-space light modes of well-defined direction and/or polarization.[16, 17, 20, 21] Indeed, it has recently been shown that holographic surface-relief plasmonic nanostructures can provide control over the (VIS/NIR) wavelength and full wavefront of light emission resulting from the point-injection of medium-energy (30 keV) electrons into the surface – the application of a structurally engineered out-coupling phase profile to the otherwise characteristically radial (cylindrically-symmetric) distribution of coherent

electron-induced radiation (surface plasmons and transition radiation) from a planar surface enables the generation, for example, of high-brightness plane wave and high-order vortex output beams.[22]

Here we demonstrate and take advantage of the low crosstalk between adjacent (even overlapping) sources of this kind, and the fact that an electron pump beam may be switched rapidly (in arbitrary, programmable sequence) among target points, to realize a multiplexed array of sources (Fig. 1) within which individual elements can be selectively pumped to generate arbitrary emission patterns 'on-demand'. We further show that the output beams of individual sources can be continuously steered within a certain angular range via fine positional adjustments of the electron beam injection point; and we demonstrate a selectively-addressable hexagonal array of sources providing for programmable modulation of emission direction and intensity using a single scanning electron beam pump.

Individual emitters were designed (after Ref. 22), for a wavelength λ = 800 nm, to generate a low-divergence, plane wave output beam at a polar angle θ = 30°: The surface-plane structure required to generate a given output beam is obtained computationally as the interference pattern between the electron-induced 'reference' field (derived from a model comprising an oscillating dipole aligned with the surface normal and positioned just above the surface, within the optical near-field) and that of the desired 'object' beam. In the present case, each source comprises 15 offset concentric oval rings around the electron injection target point, as shown in the experimental sample images inset to Fig. 2 - a geometry akin to an asymmetric plasmonic bullseye antenna[14, 23]. Samples were manufactured by focused ion beam milling in binary surface relief (etch depth 60 nm) on an optically thick (140 nm) polycrystalline gold film.

Spatial distributions of electron-induced light emission from these sources were probed in a scanning electron microscope operating in continuous-beam, fixed-spot mode at an electron energy of 30 keV and beam current of 11.4 nA, with a focal spot beam diameter ~50 nm. The system is configured with a confocal parabolic mirror to project emitted light onto a bandpass-filtered (800 ± 40 nm) nitrogen-cooled imaging CCD array. From the Cartesian CCD plane, angle-resolved maps of emission intensity are then obtained via a coordinate transformation accounting for the curvature of the mirror surface.

We first analysed the crosstalk between pairs of overlapping holographic sources oriented to emit in orthogonal (Fig. 2a) and opposing (Fig. 2b) azimuthal directions. In each case a series of samples was prepared with electron injection target point separations d ranging from zero to 30 μm. Regardless to their mutual orientation, when the two sources share a common injection point (d = 0) light is emitted equally (instrumental uncertainties aside) into both output beams, as one would expect. With the electron beam then fixed on one of the two injection points in each source pair, parasitic emission from the secondary source decreases sharply as d increases – being attenuated for both mutual

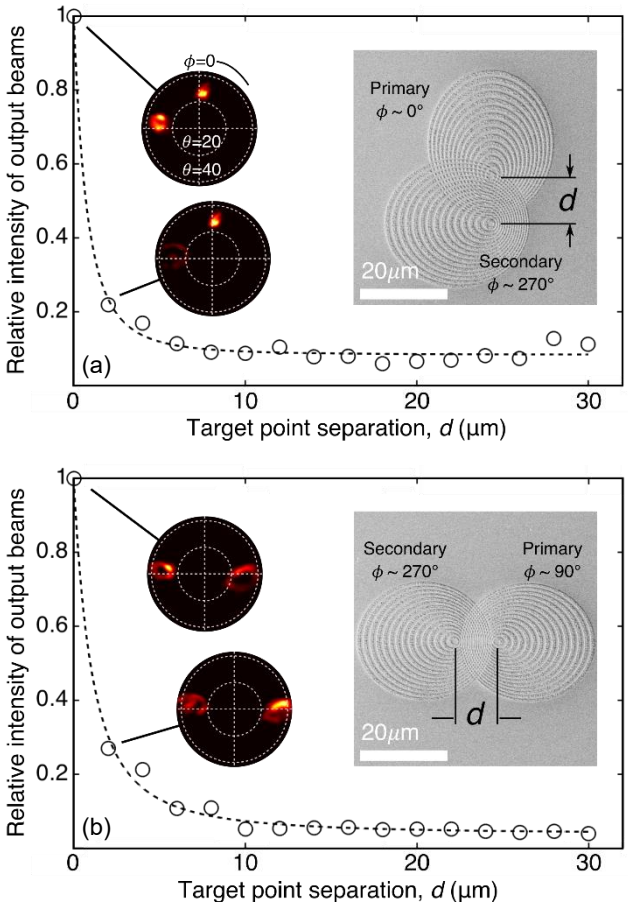

Figure 2. Relative magnitude of parasitic emission from a secondary source as a function of the separation d between its intended excitation point and the targeted electron beam injection point of the primary source for pairs of holographic sources configured to emit collimated beams at the same 800 nm wavelength and θ = 30° polar angle but (a) orthogonal and (b) opposing azimuthal angles. In each case the separation d is varied in 2 μm steps over a series of otherwise identical samples on the same gold film; insets show scanning electron microscope images of exemplar samples and angular distributions of 800 ± 20 nm light emission for d = 0 and 2 μm. [Relative intensity is evaluated as the ratio of average photon counts over pixels above half-maximum brightness for the two emission directions (±30° in azimuth angle), normalized by the ratio at d = 0 μm.]

orientations by a factor $^1/_e$ at separations d <2 μm and by an order of magnitude for separations $d \geq 6$ μm. This is in spite of the fact that the exponential surface plasmon propagation decay length for a (planar, unstructured polycrystalline) gold/vacuum interface at 800 nm is ~25 μm (Refs. 7, 8), because regardless to the strength of the reference field its wavevector distribution is almost entirely unsuitable for holographic reconstruction of the intended output beam from a positionally offset secondary mask (much as a conventional optical hologram does not reconstruct the intended image when illuminated incorrectly). In other words, while the electron-induced field still interacts with the scattering elements of an offset mask, the conditions of constructive/destructive far-field interference that produce a well-defined, directional output beam are broken – in most in-plane directions (at most azimuthal angles) electron-induced radiation no longer 'sees' the correct pattern of scattering elements.

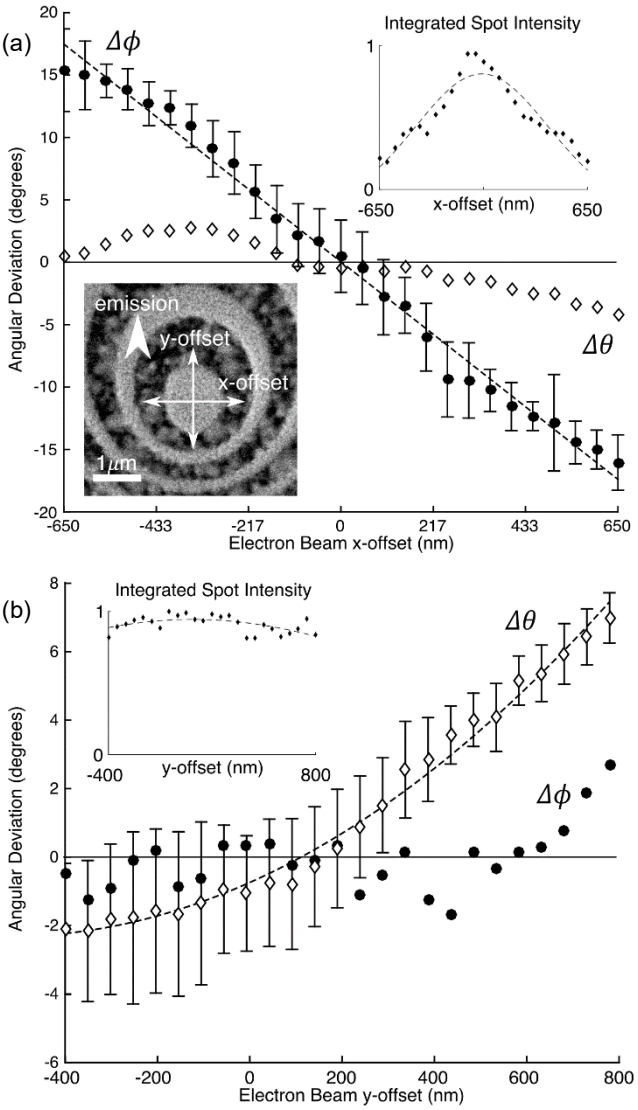

Figure 3. Steering the output beam of a single holographic source. Changes, $\Delta\theta$ and $\Delta\varphi$ respectively, in polar and azimuthal light emission angles as functions of electron injection point displacements within the central 'disc' of a single holographic source (a) perpendicular and (b) parallel to its mirror symmetry axis [in the x and y directions as defined in the scanning electron microscope image inset to panel (a)]. Injection point displacements are measured, within the constraints of instrumental resolution, relative to the target point intended by holographic design [not the geometric center of the disc]; changes in output angle are measured relative to the direction of the corresponding output beam. The insets show emission intensity integrated over the -3dB spot area as a function of x- and y-offset [intensities normalized for each directional sweep to the corresponding maximum value.]

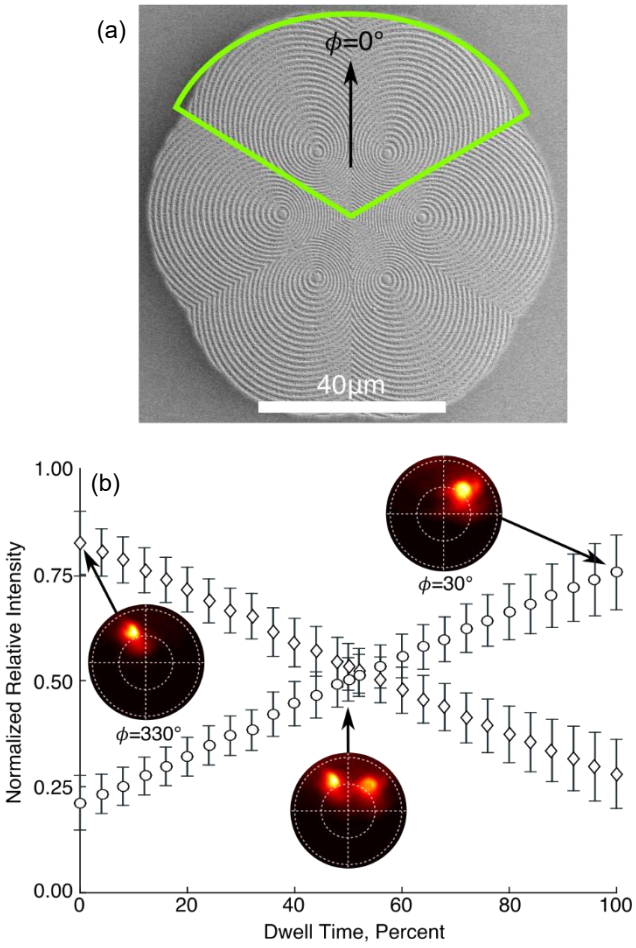

Figure 4. (a) SEM image of demonstration sample of azimuthally multiplexed hologram emitter, and (b) relative intensity of emission in two as electron beam excitation is switched between two holographic directions elements.

But the interference conditions are not broken instantaneously: somewhat as the azimuthal direction of electron-induced light emission from single plasmonic nanodisks can be tuned by adjusting the position of electron injection on the top surface of the disk,[24] here small displacements of the electron injection point within the ellipsoidal central domain of a single holographic source can be employed to steer the output beam (Fig. 3). For a single holographic source of the design presented in Fig. 2, polar and azimuthal output angles can be tuned by up to +7/-2° and ±15° respectively, by displacing the electron injection point in directions parallel and perpendicular respectively to the in-plane mirror symmetry axis of the holographic mask. (To a first approximation, θ is not expected to depend on x displacement of the electron beam, nor φ on y displacement. The deviations from zero in these data are indicative of instrumental and sample alignment inaccuracies, notably imperfect tip/tilt orientation of the parabolic mirror as discussed in Ref. 22, and imperfect rotational alignment of the sample's symmetry axis, i.e. the φ = 0 direction, with that of the mirror.) As may be expected, emission intensity is reduced as the electron beam deviates from the intended injection point (see insets to Figs. 3a and 3b), though interestingly only by ~13% when the beam is displaced parallel to the symmetry axis of the holographic structure, even at the edges of the central 'disk'; the intensity drop-off is much sharper for orthogonal 'symmetry breaking' pump beam displacements, with a loss of ~75% of intensity at the edges of the disc.

By virtue of their inherent reliance upon highly-localized excitation (i.e. inherently low crosstalk), several independent (even identical) holographic sources can be integrated over a relatively small surface area, such that a scanning electron beam may selectively address individual emitters in any sequence (with individually

tailored pump parameters of beam current, electron energy and dwell time) to rapidly modulate the optical output signal over a half-spherical field of view. Figure 4 shows a hexagonal array of six identical sources (designed for λ = 800 nm emission at θ = 30°) azimuthally oriented at 60° intervals, with a separation between nearest-neighbour electron injection target points of 16 μm. Here we have truncated and tiled the sources rather than overlapping them in the manner of Fig. 2, because with six closely spaced source patterns the density of lines increases to a point where individual lines are no longer distinguishable over much of the total area. A balance must still be struck, while keeping all electron injection points equally close to the focus of the parabolic mirror, between the density of integration and the detrimental effect of truncating individual sources (in the present case to wedge-shaped domains comprising less than half of the area of a corresponding circular holographic source) on emission brightness and sharpness (c.f. beam divergence) of the output beams. The truncated sources retain almost 90% of full-source brightness, and clear discrimination among outputs is achieved, with emission intensity in the mid-point azimuthal direction between two equally pumped neighbouring sources being at least 50% lower than in the designed beam directions, as shown by the inset to Fig. 4b at 50% dwell time. In this demonstration, for the purposes of producing a still image, the electron beam is switched (within ~5 ms) from the injection point of one source to that of the other halfway through the 20s integration time of the CCD. Depending on application though, one may switch back and forth between two sources (or among many sources), to maintain desired levels of relative time-averaged brightness, at a frequency limited only by the electron beam control and positioning system, even at picosecond timescales with laser-driven, short-pulse, electron sources[25, 26]. (Though it should be noted that as switching frequency increases, i.e. as the electron beam spends a greater proportion of time between target injection points, total brightness will decrease and, unless the beam is blanked at each switching interval, noise will increase.)

In summary, we have demonstrated experimentally that holographic free-electron-driven light sources can be assembled in close-packed multiplexed arrays, with minimal crosstalk between adjacent elements (i.e. without any discernible parasitic output beams being generated by elements adjacent to the one being pumped). These can be programmably addressed, taking advantage of the highly-localized and positionally-agile nature of a focused electron-beam pump, to generate selected patterns of light emission.

The demonstration here employs a single electron beam (in a scanning electron microscope) to selectively pump one light source at a time among an array of holographic emitters, each of which is designed to generate a directional near-infrared plane-wave output beam. But neither of these aspects represents a constraint on application: indeed, it has been shown[22] that holographic surface-relief structures can be engineered to produce complex wavefronts such as high-order vortex beams; and in the context of flat-panel field-emission and surface-conduction electron-emitter display (FED, SED) technologies, large addressable arrays of microscopic ballistic electron sources operating at acceleration voltages >10 kV are well-known.[27] Neither is the spectrally broad nature of the underlying emission mechanisms necessarily a drawback: while sources are designed to operate at a particular wavelength (800 nm in the present case), they are diffractive and will decouple longer/shorter wavelengths at higher/lower polar angles (with decreasing efficiency as detuning from the design wavelength increases[22]). One may thus envisage a chip-scale, dynamically programmable array of holographic light sources, each designed to emit a different wavelength and/or wavefront profile in different polar and/or azimuthal directions, and each pumped by a dedicated electron source. Such a device would offer considerable applications potential, for example, in optical tweezer and micro-spectroscopy applications.

Moreover, on the basis that the output beam direction for individual holographic light sources varies continuously with electron pump beam position on the central disk, such structures may be engaged as sensors of electron (or more generally, charged particle) beam pointing stability, with nanometric injection point displacements manifested as output light beam displacements on a positon-sensitive photodetector.

This work was supported by the Engineering and Physical Sciences Research Council, UK [Project EP/M009122/1], and the Singapore Ministry of Education [grant MOE2011-T3-1-005]. Following a period of embargo, the data from this paper can be obtained from the University of Southampton research repository http://doi.org/10.5258/SOTON/D0361.

1. F. J. García de Abajo, Rev. Mod. Phys. **82**, 209-275 (2010).
2. V. L. Ginzburg and I. M. Frank, J. Phys. (USSR) **9**, 353-362 (1945).
3. M. V. Bashevoy, F. Jonsson, A. V. Krasavin, N. I. Zheludev, Y. Chen and M. I. Stockman, Nano Lett. **6** (6), 1113-1115 (2006).
4. J. T. van Wijngaarden, E. Verhagen, A. Polman, C. E. Ross, H. J. Lezec and H. A. Atwater, Appl. Phys. Lett. **88**, 221111 (2006).
5. S. J. Smith and E. M. Purcell, Phys. Rev. **92** (4), 1069 (1953).
6. J. So, K. F. MacDonald and N. I. Zheludev, Appl. Phys. Lett. **104**, 201101 (2014).
7. M. V. Bashevoy, F. Jonsson, K. F. MacDonald, Y. Chen and N. I. Zheludev, Opt. Express **15** (18), 11313-11320 (2007).
8. M. Kuttge, E. J. R. Vesseur, J. Verhoeven, H. J. Lezec, H. A. Atwater and A. Polman, Appl. Phys. Lett. **93**, 113110 (2008).
9. J. Nelayah, M. Kociak, O. Stéphan, F. J. García de Abajo, M. Tencé, L. Henrard, D. Taverna, I. Pastoriza-Santos, L. M. Liz-Marzán and C. Colliex, Nat. Phys. **3** (5), 348-353 (2007).
10. M. Bosman, V. J. Keast, M. Watanabe, A. I. Maaroof and M. B. Cortie, Nanotech. **18**, 165505 (2007).
11. V. Myroshnychenko, J. Nelayah, G. Adamo, N. Geuquet, J. Rodríguez-Fernández, I. Pastoriza-Santos, K. F. MacDonald, L. Henrard, L. M. Liz-Marzán, N. I. Zheludev, M. Kociak and F. J. García de Abajo, Nano Lett. **12**, 4172−4180 (2012).

12. A. I. Denisyuk, F. Jonsson, K. F. MacDonald, N. I. Zheludev and F. J. García de Abajo, Appl. Phys. Lett. **92**, 093112 (2008).
13. C. Xiao, Z. Li, H. Guthrey, J. Moseley, Y. Yang, S. Wozny, H. Moutinho, B. To, J. J. Berry, B. Gorman, Y. Yan, K. Zhu and M. Al-Jassim, J. Phys. Chem. C **119**, 26904-26911 (2015).
14. C. I. Osorio, T. Coenen, B. J. M. Brenny, A. Polman and A. F. Koenderink, ACS Photon. **3**, 147-154 (2015).
15. A. C. Atre, B. J. M. Brenny, T. Coenen, A. García-Etxarri, A. Polman and J. A. Dionne, Nat. Nanotech. **10**, 429-436 (2015).
16. G. Adamo, K. F. MacDonald, Y. H. Fu, C.-M. Wang, D. P. Tsai, F. J. García de Abajo and N. I. Zheludev, Phys. Rev. Lett. **103**, 113901 (2009).
17. G. Adamo, J. Y. Ou, J. So, S. D. Jenkins, F. De Angelis, K. F. MacDonald, E. Di Fabrizio, J. Ruostekoski and N. I. Zheludev, Phys. Rev. Lett. **109**, 217401 (2012).
18. J. Ge and Y. Yin, Angew. Chem Int. Edit. **50**, 1492 – 1522 (2011).
19. N. I. Zheludev and E. Plum, Nat. Nanotech. **11**, 16-22 (2016).
20. A. I. Denisyuk, G. Adamo, K. F. MacDonald, J. Edgar, M. D. Arnold, V. Myroshnychenko, M. J. Ford, F. J. García de Abajo and N. I. Zheludev, Nano Lett. **10**, 3250–3252 (2010).
21. T. Coenen, E. J. R. Vesseur, A. Polman and A. F. Koenderink, Nano Lett. **11** (9), 3779-3784 (2011).
22. G. Li, B. Clarke, J. So, K. F. MacDonald and N. I. Zheludev, Nat. Commun. **7**, 13705 (2016).
23. H. J. Lezec, A. Degiron, E. Devaux, R. A. Linke, L. Martin-Moreno, F. J. Garcia-Vidal and T. W. Ebbesen, Science **297** (5582), 820-822 (2002).
24. T. Coenen, F. Bernal Arango, A. Femius Koenderink and A. Polman, Nat. Commun. **5**, 3250 (2014).
25. V. A. Lobastov, R. Srinivasan and A. H. Zewail, Proc. Natl. Acad. Sci. USA **102** (20), 7069–7073 (2005).
26. A. Feist, N. Bach, N. Rubiano da Silva, T. Danz, M. Möller, K. E. Priebe, T. Domröse, J. G. Gatzmann, S. Rost, J. Schauss, S. Strauch, R. Bormann, M. Sivis, S. Schäfer and C. Ropers, Ultramicroscopy **176**, 63-73 (2017).
27. S. Itoh, M. Tanaka and T. Tonegawa, J. Vac. Sci. Technol. B **22** (3), 1362-1366 (2004).